J. Astrophys. Astr. (2009) **30,** 1–36

The Fate of Dwarf Galaxies in Clusters and the Origin of Intracluster Stars

Paramita Barai*, William Brito & Hugo Martel
Département de physique, de génie physique et d'optique, Université Laval, Québec City, Québec, G1K 7P4, Canada.
**e-mail: paramita.barai.1@ulaval.ca*

Received 2008 March 4; accepted 2009 March 13

Abstract. The main goal of this paper is to compare the relative importance of destruction by tides *vs.* destruction by mergers, in order to assess if tidal destruction of galaxies in clusters is a viable scenario for explaining the origin of intracluster stars. We have designed a simple algorithm for simulating the evolution of isolated clusters. The distribution of galaxies in the cluster is evolved using a direct gravitational N-body algorithm combined with a subgrid treatment of physical processes such as mergers, tidal disruption, and galaxy harassment. Using this algorithm, we have performed a total of 148 simulations. Our main results are:

- destruction of dwarf galaxies by mergers dominates over destruction by tides, and
- the destruction of galaxies by tides is sufficient to explain the observed intracluster light in clusters.

Key words. Cosmology—galaxies: clusters, dwarfs, interactions—methods: numerical.

1. Introduction

Dwarf galaxies (DGs) are defined as low-mass (10^7–10^9 $M_\odot$) galaxies having an absolute magnitude fainter than $M_B \sim -16$ mag, or $M_V \sim -18$ mag (Grebel 2001), have low surface brightness and low metallicity. They are the most numerous galaxies occurring in the Universe. A majority of galaxies in the local group are DGs (Mateo 1998). DGs have been seen in observations of nearby galaxy clusters, Coma (Thompson & Gregory 1993; Bernstein *et al.* 1995), Virgo (Sandage *et al.* 1985; Lee *et al.* 2003), Fornax (Bothun *et al.* 1991; Drinkwater *et al.* 2003), Centaurus (Mieske *et al.* 2007), and several galaxy groups (Karachentseva *et al.* 1985; Côté *et al.* 1997; Cellone & Buzzoni 2005).

The diffuse intracluster light (ICL) observed in clusters of galaxies is produced by stars, usually of low surface brightness, located outside individual galaxies but within the cluster and associated with the cluster potential. The first mention of IC light was made by Zwicky (1951). Since then, several observations have detected diffuse ICL in many galaxy cluster systems (Arnaboldi 2004; Gonzalez *et al.* 2005; Mihos *et al.* 2005;

Krick *et al.* 2006). The idea of IC globular clusters was proposed by West *et al.* (1995). Later on, distinct IC stars were observed (Arnaboldi *et al.* 2003; Gal-Yam *et al.* 2003; Gerhard *et al.* 2005), including globular clusters, red giant stars, and SN Ia. The origin and evolution of the IC stars and diffuse ICL are not well constrained at present.

The most popular formation mechanism of IC population is stripping of stars from cluster galaxies by gravitational tides, fast encounters between galaxies, and tidal interactions between colliding and merging galaxies (Miller 1983; Gregg & West 1998). From observations and cosmological simulations, at $z = 0$ at least 10–20% of all stars in a cluster are unbound to any one galaxy (e.g., Aguerri *et al.* 2005). The fraction of stars in ICL increases with mass of the clusters, and increases with density of environment: from loose groups ($< 2\%$, Castro-Rodriguez *et al.* 2003), to Virgo-like (10%, Feldmeier *et al.* 2004b; Zibetti *et al.* 2005) and rich clusters ($\sim$20% or higher, Tyson & Fischer 1995; Feldmeier *et al.* 2004a; Krick & Bernstein 2007). In the cores of dense and rich clusters (like Coma) the local ICL fraction can be as high as 50% (Bernstein *et al.* 1995).

In numerical studies of ICL production in clusters, there is always a trade-off between having good resolution or good statistics. Napolitano *et al.* (2003); Willman *et al.* (2004); Sommer-Larsen *et al.* (2005), and Rudick *et al.* (2006) simulate either one cluster or a few clusters, so even though their simulations have high resolution, they have poor statistics, in the sense that the cluster(s) they are simulating might not be representative of the whole cluster population. On the other extreme, Murante *et al.* (2004) simulate a very large cosmological volume, containing a statistically significant sample of clusters. Such large simulations, however, cannot resolve the scale of dwarf galaxies. Our goal is to have it both ways: achieving good statistics while resolving the processes responsible for destroying dwarf galaxies. This is achieved by combining large-scale cosmological simulations with a semi-analytical treatment of mergers and tidal disruption.

The main objective of our present work is to determine if DGs in clusters are more prone to destruction by tides or to destruction by mergers. This determination is then used to predict the contribution of DGs to the origin of IC stars. The DGs in a cluster can be tidally disrupted (by the field of a more massive galaxy or by the background halo) or the DGs can be destroyed when they merge with another galaxy. The impact of these two destruction mechanisms on the ICL is radically different. In the case of tidal disruption, the process contributes to IC stars in the cluster. In the case of merger, the DG is absorbed by a more massive galaxy, and there is essentially no contribution to the IC stars.

We perform numerical simulations of isolated clusters of galaxies, in order to examine which method of dwarf galaxy destruction is dominant, and how the process depends on environmental factors. We identify six possible outcomes for our simulated galaxies:

(1) the galaxy merges with another galaxy,
(2) the galaxy is destroyed by the tidal field of a larger galaxy but the fragments accrete onto that larger galaxy,
(3) the galaxy is destroyed by tides and the fragments are dispersed in the intracluster medium (ICM), contributing to the intracluster light,
(4) the galaxy is destroyed by the tidal field of the background halo,

(5) the galaxy survives to the present, and
(6) the galaxy is ejected from the cluster.

We designed a simple algorithm to follow the evolution of galaxies in an isolated cluster. The gravitational interaction between galaxies is calculated by a direct N-body algorithm. The other physical mechanisms governing the possible outcomes (mergers, tidal disruption, accretion, etc.) of the simulated galaxies are treated as 'subgrid physics', and are incorporated in the algorithm using a semi-analytical method. In the present work, we use this algorithm to simulate the evolution of isolated galaxy clusters, i.e., we assume that the cluster has already formed with its constituent galaxies in place, and it is neither accreting nor merging, except in section 4.7 where we consider accretion.

The remainder of this paper is organized as follows: In section 2, we outline the numerical model for our galaxy clusters. The methodology of our simulations is described in section 3. The results are presented in section 4. We discuss the implications of our main goals in section 5, and give our conclusions in section 6.

2. The numerical method

2.1 *The basic PP algorithm*

We treat the system as an isolated cluster consisting of N galaxies of mass m_i, radius s_i, and internal energy U_i, orbiting inside a background halo of uncollapsed dark matter and gas. We assume that the halo is spherically symmetric, and its radial density profile $\rho_{\rm halo}(r)$ does not evolve with time (hence, we are neglecting infall motion that would result from cooling flows). Furthermore, we assume that the halo is stationary: it does not respond to the forces exerted on it by the galaxies, and therefore its center remains fixed at a point that we take to be the origin. In section 4.7, we relax the assumption of an isolated cluster, and consider mass growth of the cluster with time, which can happen due to accretion.

We represent each galaxy by *one single particle* of mass m_i. The 'radius' s_i of the galaxy and its 'internal energy' U_i are internal variables that only enter in the treatment of the subgrid physics described in section 2.4. Our motivation for using this approach is the following: To simulate the destruction of dwarf galaxies by tides, it would seem more appropriate to simulate each galaxy using many particles. Supposing, however, that it takes at least 100 particles to properly resolve a dwarf galaxy experiencing tidal destruction, as the galaxies in our simulations cover three orders of magnitude in mass, the most massive ones would be represented by 100,000 particles. Even though the dwarf galaxies are much more numerous than the massive ones, the total number of particles would be above one million. This raises the following issues:

- With the use of tree codes, an $N = 10^6$-particle simulation is not considered prohibitive anymore. However, (1) our model has several free parameters, so we have a full parameter-space to study, and (2) one single cluster is not statistically significant, so for each combination of parameters we need to perform several simulations. For this paper, we performed 148 simulations. Doing 148 million-particle simulations would start to be computationally expensive.
- We could use unequal-mass particles, so that the most massive galaxies would not be represented by large number of particles. This is usually not a good idea.

N-body simulations with particles having widely different masses are known to suffer from all sorts of instability problems, which often require special algorithms to deal with. The approach we are considering here is more practical.

- In this paper, we consider isolated clusters. In a forthcoming paper (Brito *et al.* 2008), we will present simulations of a cosmological volume containing at least 100 clusters. The number of particles would then reach 100 million, and we would still need to explore the parameter space. This would be computationally very expensive. We will solve this problem using single-particle galaxies combined with a treatment of subgrid physics. The simulations presented in this paper can be seen as a test-bed for this approach.

The relatively small number of particles in our simulations (typically less than 1000) enable us to use a direct, particle–particle (PP) algorithm, which is the simplest of all N-body algorithms. We took a standard PP code, which evolves a system of N gravitationally interacting particles using a second-order Runge–Kutta algorithm. We modified the original algorithm to include the interaction with the background halo, and we added several modules to deal with the subgrid physics. In this modified algorithm, the number of particles N can vary, as they merge, are destroyed by tides, or escape the cluster.

2.2 *Gravitational interactions*

The acceleration of particle i (or galaxy i) is given by

$$\mathbf{a}_i = -G \sum_{j \neq i} \frac{m_j(\mathbf{r}_i - \mathbf{r}_j)}{\left(|\mathbf{r}_i - \mathbf{r}_j|^2 + \epsilon^2\right)^{3/2}} - \frac{G M_{\rm halo}(r_i)\mathbf{r}_i}{(r_i^2 + \epsilon^2)^{3/2}}\,, \tag{1}$$

where $\mathbf{r}_i$ and $\mathbf{r}_j$ are the positions of particles i and j, respectively, m_j is the mass of particle j, $M_{\rm halo}(r_i)$ is the mass of the background halo inside $r = r_i$, G is the gravitational constant, and ϵ is the softening length. This assumes that the background cluster halo is spherically symmetric and centered at the origin. In our PP algorithm, this expression is evaluated directly, by summing over all particles $j \neq i$. The softening length ϵ is chosen to be smaller than the initial radius of the smallest galaxies (see section 3.2 for the determination of the initial radius). Our results are not sensitive to the value of ϵ, as long as it is smaller than the radii of the smallest galaxies.

We evolve the system forward in time using a second-order Runge–Kutta algorithm. The timestep Δt is calculated using:

$$\Delta t = \min_i (\Delta t)_i\,, \qquad (\Delta t)_i = \min\left[\frac{\epsilon}{|\mathbf{v}_i|}, \left(\frac{\epsilon}{|\mathbf{a}_i|}\right)^{1/2}\right], \tag{2}$$

where $\mathbf{v}_i$ is the velocity of particle i, and we take the smallest value of $(\Delta t)_i$ to be the timestep Δt.

2.3 *The cluster halo density profile*

We consider two different types of density profile of the background halo of a cluster, $\rho_{\rm halo}(r)$: the β profile, and the NFW profile.

In the first case, we assume that the dark matter in the background halo follows a similar density distribution as the observed intracluster gas. A single β-model (isothermal) density profile is used for the gas (e.g., King 1962; Cavaliere & Fusco-Femiano 1976; Makino *et al.* 1998),

$$\rho_{\rm gas}(r) = \rho_0 \left[1 + \left(\frac{r}{r_c}\right)^2\right]^{-3\beta/2}, \tag{3}$$

where ρ_0 is the central density and r_c is the core radius. The values of ρ_0, r_c and β are taken from Piffaretti & Kaastra (2006), which give the gas density parameters for 16 nearby clusters. The halo density is then obtained by scaling the gas density with the universal ratio of matter (dark + baryonic) to baryons, $\rho_{\rm halo} = \rho_{\rm DM} + \rho_{\rm gas} = \rho_{\rm gas}\Omega_M/\Omega_b$, where Ω_M and Ω_b are the present matter (baryons + dark matter) density parameter and baryon density parameter, respectively. This assumes that the cluster baryon mass fraction follows the cosmic value of Ω_b/Ω_M, which is expected to be generally true (e.g., White *et al.* 1993; Ettori 2003), although precise estimations of cluster baryon content have shown deviations from the universal value (Gonzalez *et al.* 2007, and references therein).

In the second case, we consider that the distribution of gas and dark matter in the background halo both follow analytical models of the dark matter density having a functional form:

$$\rho_{\rm DM}(r) = \frac{\rho_s}{(r/r_s)(1 + r/r_s)^2} \tag{4}$$

(Navarro *et al.* 1997). Here, ρ_s is a scaling density and r_s is a scale length. The NFW profile is often parametrized in terms of a concentration parameter c. The parameters ρ_s and r_s are then given by:

$$\begin{aligned}\rho_s &= \frac{200c^3\rho_{\rm crit}(z)}{3[\ln(1+c) - c/(1+c)]} \\ &= \frac{25H^2(z)c^3}{\pi G[\ln(1+c) - c/(1+c)]},\end{aligned} \tag{5}$$

$$r_s = \frac{r_{200}}{c}, \tag{6}$$

where $\rho_{\rm crit}(z) = 3H^2(z)/8\pi G$ is the critical density at formation redshift z, and r_{200}, the virial radius, is the radius of a sphere whose mean density is $200\rho_{\rm crit}$ (200 times the critical density of the Universe at the epoch of formation). After scaling, the halo density profile is $\rho_{\rm halo} = \rho_{\rm DM}\Omega_M/(\Omega_M - \Omega_b)$.

Once we have chosen a particular density profile, the density is integrated to get the background cluster halo mass as:

$$M_{\rm halo}(r) = \int_0^r 4\pi x^2 \rho_{\rm halo}(x)dx. \tag{7}$$

This is the mass that enters in the last term of equation (1). Since the density profiles we consider do not have an outer edge where $\rho_{\rm halo} = 0$, we truncate the cluster background

halo at a maximum halo radius $R_{\rm halo}^{\rm max} = 5$ Mpc. Equation (7) is then solved numerically, to build an interpolation table for r in the range $\left[0,\ R_{\rm halo}^{\rm max}\right]$ that is then used by the code.

2.4 *The subgrid physics*

As mentioned in section 1, there can be six possible physical outcomes for our simulated cluster galaxies. In the following subsections, we describe the associated subgrid physics for each mechanism we use in our simulations. The possible outcomes are:

- the galaxy merges with another galaxy (section 2.4.1),
- the galaxy is destroyed by the tidal field of a larger galaxy but the fragments accrete onto that larger galaxy (section 2.4.4),
- the galaxy is destroyed by tides of a larger galaxy and the fragments are dispersed in the intracluster medium (section 2.4.3),
- the galaxy is destroyed by the tidal field of the background halo (section 2.4.3),
- the galaxy survives to the present (i.e., it is not destroyed by any process), and
- the galaxy is ejected from the cluster (section 2.4.5).

We describe our approach of simulating galaxy harassment in section 2.4.2.

2.4.1 *Encounter: Merger*

We simulate a pair of galaxies colliding (or synonymously, having an encounter) and the further consequences (e.g., merging) in the following way. An encounter is accounted for when two galaxies i and j, of radii s_i and s_j, overlap such that the center of the galaxy j is inside the galaxy i. Numerically the criterion is $r_{ij} < s_i$, where $r_{ij} = |\mathbf{r}_i - \mathbf{r}_j|$ is the distance between the centers of the galaxies. If $\mathbf{v}_i$ and $\mathbf{v}_j$ are the velocities of galaxies i and j, the center of mass velocity of the pair is $\mathbf{v}_{\rm cm} = (m_i\mathbf{v}_i + m_j\mathbf{v}_j)/(m_i + m_j)$. The kinetic energy in the center-of-mass rest frame is:

$$K_{ij} = \frac{1}{2}m_i|\mathbf{v}_i - \mathbf{v}_{\rm cm}|^2 + \frac{1}{2}m_j|\mathbf{v}_j - \mathbf{v}_{\rm cm}|^2. \tag{8}$$

The gravitational potential energy of the pair is:

$$W_{ij} = -\frac{Gm_im_j}{r_{ij}}. \tag{9}$$

Even though we are treating each galaxy as a single particle, in reality a galaxy is a gravitationally bound system with an internal kinetic energy and a potential energy, and these energies must be included in the total energy of the interacting pair of galaxies. Considering a galaxy as a bound virialized system its internal energy is:

$$U_i = U_{\rm potential} + U_{\rm kinetic} = \frac{U_{\rm potential}}{2} = -\frac{\zeta Gm_i^2}{2s_i}, \tag{10}$$

where ζ is a geometrical factor which depends on the mass distribution in the galaxies. Throughout this paper, we assume $\zeta = 1$ (see Appendix).

We then compute the total energy of the galaxy pair (in the center of mass frame) as:

$$E_{ij} = K_{ij} + W_{ij} + U_i + U_j. \tag{11}$$

If $E_{ij} \leq 0$, i.e., the system is bound, we then allow the galaxies to merge to form a single galaxy of mass $m_{\rm merge} = m_i + m_j$. To compute its radius, we assume that energy is conserved, hence the total energy E_{ij} in the center-of-mass rest frame is all converted into the internal energy of the merger remnant. Its radius is then computed from equation (10),

$$s_{\rm merged} = -\frac{\zeta G m_{\rm merge}^2}{2U_{\rm merge}} = \frac{\zeta G(m_i + m_j)^2}{2|E_{ij}|}\,. \tag{12}$$

The position and velocity of this merged object are set to those of the center-of-mass values of the galaxy pair before merger, in order to conserve momentum.

2.4.2 *Encounter: Galaxy harassment*

In a high-speed encounter the two interacting galaxies come into contact for a brief amount of time. The galaxies might survive a merger or tidal disruption, but the encounter adds some internal energy into them, making them less bound. We refer to this process as *Galaxy Harassment*. This process has been originally suggested as a possible explanation for the origin of the morphology–density relation in clusters (Moore *et al.* 1996). We incorporate galaxy harassment in our algorithm by increasing the radius (or the internal energy) of a galaxy when it experiences a non-merger encounter. This enlargement makes a galaxy more prone to tidal disruption at the next encounter.

In equation (11), if $E_{ij} > 0$, i.e., the system is not bound, then the galaxies in our simulation do not merge in the collision. Rather a part of the kinetic energy of the galaxies is converted into internal energy, making the collision inelastic. We assume that an equal amount of energy is transfered to each galaxy. Denoting the energy transfered as ΔE, the kinetic energy of the pair decreases by ΔE, while the internal energy of each galaxy increases by $\Delta E/2$. We assume:

$$\frac{\Delta E}{2} = \eta \min(|U_i|, |U_j|)\,, \tag{13}$$

where η is an energy transfer efficiency whose value is taken as $\eta = 0.2$. The internal energies of the two galaxies after the encounter are $U_i^{\rm after} = U_i^{\rm before} + \Delta E/2$ and $U_j^{\rm after} = U_j^{\rm before} + \Delta E/2$, respectively. By choosing $\eta < 1$, we are ensuring that the internal energy of each galaxy remains negative, that is, the transfer of energy does not unbind the galaxies. We recalculate the velocities $\mathbf{v}_i$ and $\mathbf{v}_j$ after collision while conserving momentum, assuming that only the magnitudes of velocity change, the directions remaining the same. We recalculate the size of each galaxy in the pair using equation (12),

$$s_i^{\rm after} = \frac{\zeta G m_i^2}{2|U_i^{\rm after}|}\,, \qquad s_j^{\rm after} = \frac{\zeta G m_j^2}{2|U_j^{\rm after}|}. \tag{14}$$

While allowing a size increase of the galaxies according to equations (12) and (14), we also considered a size cut-off. We assumed that the galaxies could grow only up to a maximum size given by the size of the largest galaxy at the beginning of the simulation.

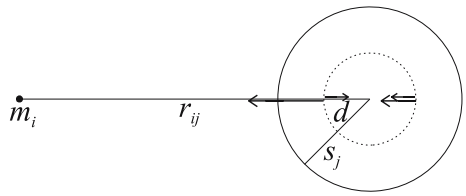

Figure 1. Calculation of the effects of tides caused by a galaxy of mass m_i on a galaxy of mass m_j and radius s_j. The two largest arrows show the gravitational accelerations caused by galaxy i; the two smallest arrows show the accelerations caused by galaxy j. See section 2.4.3 for details.

2.4.3 *Tidal disruption: Intracluster stars*

We consider two possible sources of external gravitation for the tidal disruption of a galaxy j: another galaxy i, or the background cluster halo. The tidal force on a galaxy due to the gravitational field of the external source is meaningful only if the galaxy lies entirely on one side of the external source, when the tides are directed radially outwards tending to tear apart the galaxy. Our calculation of the tidal field caused by a galaxy i of mass m_i is illustrated in Fig. 1. The galaxies i and j are separated by a distance r_{ij}. We calculate the resultant fields between two diametrically opposite points inside galaxy j, located at a radial distance $d \leq s_j$ along the line joining the centers of the two galaxies. The two small and two large arrows in Fig. 1 indicate the gravitational field (or acceleration) at the opposite points caused by galaxy j (self-gravity) and by galaxy i (external source of gravitation), respectively. The magnitude of the tidal field is given by the difference between the gravitational field caused by galaxy i at the two opposite points,[1]

$$a_{\rm tide}^{\rm galaxy} = \frac{Gm_i}{(r_{ij}-d)^2} - \frac{Gm_i}{(r_{ij}+d)^2}. \tag{15}$$

The gravitational field caused by galaxy j (two small arrows in Fig. 1) is directed radially inwards and acts opposite to the tides, tending to keep the galactic mass inside radius d intact. The difference between that self-gravitational field at the two opposite points is:

$$a_{\rm grav} = \frac{2Gm_j(d)}{d^2}, \tag{16}$$

where $m_j(d)$ is the mass of galaxy j inside radius d. When $a_{\rm tide}^{\rm galaxy} = a_{\rm grav}$, then the tides will exceed self-gravity at radii larger than d, while self-gravity will exceed the tides at smaller radii. Thus the layers of galactic mass located between radii d and s_j would become unbound, while the ones located inside radius d would remain bound. Hence, the galaxy would be partly disrupted. In our code, we simplify things by using an 'all-or-nothing' approach. A galaxy is either totally disrupted, or not disrupted at all. We consider that a galaxy is disrupted if half of its mass or more becomes unbound. If we assume an isothermal sphere density profile (as in Appendix), then the half-mass

[1]This reduces to the well-known form $a_{\rm tide}^{\rm galaxy} \propto d/r_{ij}^3$ in the limit $d \ll r_{ij}$, but we do not make this approximation here.

radius is given by $d = s_j/2$. This is the value of d we use in equations (15) and (16). The criterion of tidal destruction then becomes $a_{\rm tide}^{\rm galaxy}(d) \geq a_{\rm grav}(d)$, with $d = s_j/2$.

We also consider tidal disruption by the background cluster halo, but only if $r_j > s_j$ (that is, the galaxy does not overlap with the center of the halo). The magnitude of tidal field due to the cluster halo is:

$$a_{\rm tide}^{\rm halo} = \frac{GM_{\rm halo}(r_j - d)}{(r_j - d)^2} - \frac{GM_{\rm halo}(r_j + d)}{(r_j + d)^2}\,, \tag{17}$$

where $M_{\rm halo}(r)$ is given by equation (7). If $a_{\rm tide}^{\rm halo}(d) \geq a_{\rm grav}(d)$, with $d = s_j/2$, galaxy j is tidally destroyed by the gravitational field of the halo.

When galaxy j is considered to have been tidally destroyed by another galaxy i, the fragments of the disrupted galaxy might accrete onto galaxy i (section 2.4.4), or they might be dispersed into the ICM when $E_{ij} > 0$ (E_{ij} being the total energy of the galaxy pair given by equation 11). For tidal destruction by the cluster halo the disrupted fragments are always dispersed into the ICM. In both cases, the destroyed galaxy is removed from the list of existing particles. The code keeps track of the amount of mass added to the ICM (in the form of IC stars) by tidal disruption. This quantity is initialized to zero at the beginning of the simulation, and every time a galaxy is tidally destroyed with its fragment dispersed, the mass of that galaxy is added up to the total mass added to the ICM.

2.4.4 *Tidal disruption: Accretion*

We consider a possibility of accretion of the fragments of a tidally disrupted galaxy onto the galaxy causing the tides. This happens for the case of tidal disruption due to galaxies only (if the disruption is caused by the background cluster halo, the fragments are always dispersed as IC stars). This situation occurs when the conditions $a_{\rm tide}^{\rm galaxy} > a_{\rm grav}$ and $E_{ij} \leq 0$ are both satisfied (see section 2.4.3). The tidally disrupted galaxy accretes onto the more massive galaxy. The mass of the bigger galaxy increases from m_i to $m_i + m_j$. Thus a tidal disruption followed by accretion is similar to a merger (section 2.4.1), but these events are counted separately.

2.4.5 *Ejection*

When a galaxy ventures at distances larger than the cluster halo truncation radius $R_{\rm halo}^{\rm max}$ (see section 2.3), we consider that this galaxy has escaped from the cluster, and we remove it from the list. If we kept that galaxy, it might eventually return to the cluster. But in reality the universe contains many clusters, and a galaxy that moves sufficiently far away from one cluster will eventually feel the gravitational influence of other clusters, something that our algorithm, which simulates an isolated cluster, does not take into account. As we shall see, the ejection of galaxies from a cluster is quite uncommon in our simulations.

3. The simulations

3.1 *Cosmological model*

We consider a ΛCDM model with the present matter density parameter, $\Omega_M = 0.241$, baryon density parameter, $\Omega_b = 0.0416$, cosmological constant, $\Omega_\Lambda = 0.759$, Hubble

constant, $H_0 = 73.2\,\mathrm{km\,s^{-1}Mpc^{-1}}$ ($h = 0.732$), primordial tilt, $n_s = 0.958$, and CMB temperature, $T_{\mathrm{CMB}} = 2.725\,\mathrm{K}$, consistent with the results of *WMAP3* (Spergel *et al.* 2007). Even though the simulations presented in this paper are not 'cosmological' (we simulate isolated, virialized clusters), the particular choice of cosmological model enters the picture twice: in the determination of the radii of galaxies (see next section), and in the calculation of the elapsed time between the initial and final redshifts of the simulation.

In each simulation a cluster is evolved from $z = 1$ to the present ($z = 0$). We assume that the cluster will not experience any major merger during this period, and that, therefore, it is a good approximation to treat it as isolated. For our ΛCDM model, this represents a total evolutionary time of 7.63 Gyr.

3.2 *Initial conditions*

To set the initial conditions of our simulations, we need to determine the initial mass m, radius s, position $\mathbf{r}$, and velocity $\mathbf{v}$ of each galaxy. To determine the mass, we first assume that the luminosities of galaxies are distributed according to the Schechter luminosity function (Schechter 1976),

$$\phi(L)dL = \phi^* \left(\frac{L}{L^*}\right)^{\alpha} e^{-L/L^*} \frac{dL}{L^*}\,. \tag{18}$$

Here we use $L^* = 3.097 \times 10^{10}\,\mathrm{L_\odot}$ (corresponding to absolute magnitude $M^*_{b_J} = -20.07$), and $\alpha = -1.28$, which is appropriate for galaxies located in clusters (De Propris *et al.* 2003). This luminosity function spans over $-22.5 < M_{b_J} < -15$. While it might be reasonable to assume fixed values of L^* and α, the value of ϕ^* most likely varies amongst clusters. So we normalize equation (18) by imposing that, in each cluster, there are N_0 galaxies with luminosities $L > L_0$. We use $N_0 = 25$, and $L_0 = 0.2L^*$ (corresponding to $M_b = -19$) (Lewis *et al.* 2002). We select the luminosities using a Monte Carlo rejection method. We then assume a constant mass-to-light ratio $\Upsilon = 193\,\mathrm{h\ M_\odot/L_\odot} = 73$ (Brainerd & Specian 2003), and convert the luminosities to masses. The Schechter function spans up to a maximum mass $M_{\mathrm{max}} = 220 \times 10^{11}\mathrm{M_\odot}$. To generate the dwarf galaxies, the same Schechter function is extrapolated up to a minimum mass $M_{\mathrm{min}} = 1 \times 10^{9}\mathrm{M_\odot}$.

We take the radius s of each galaxy to be equal to the virial radius r_{200} (radius containing matter with 200 times the mean density of the Universe at the epoch of galaxy formation) corresponding to the galaxy mass $m = M_{200}$ using:

$$M_{200} = \frac{800\pi}{3} r_{200}^3 \bar{\rho} (1 + z_{\mathrm{coll}})^3. \tag{19}$$

Here, $\bar{\rho} = \rho_{\mathrm{crit}}\Omega_M = 3H_0^2\Omega_M/8\pi G$ is the mean matter density in the present universe, and z_{coll} is the redshift of collapse when the galaxy formed. To obtain z_{coll}, we use a simple spherical collapse model. First, by filtering the power spectrum for our ΛCDM model, we calculate the standard deviation $\sigma(m)$ of the linear density contrast $\delta = (\rho - \bar{\rho})/\bar{\rho}$ at the mass scale m. The distribution of the values of δ is then given by a Gaussian,

$$\mathcal{P}(\delta) \propto \exp\left(-\frac{\delta^2}{2\sigma^2}\right). \tag{20}$$

We pick randomly a present density contrast $\delta_0 = \delta(z = 0)$ from this distribution, using a Monte Carlo rejection method, and solve the following equation to get the collapse redshift $z_{\rm coll}$,

$$\Delta_c = \delta_0 \frac{\delta_+(z_{\rm coll})}{\delta_+(0)}\,, \tag{21}$$

where $\delta_+(z)$ is the linear growing mode (for $\Lambda \neq 0$ models, see, e.g., Martel 1991). Here, $\Delta_c = 3(12\pi)^{2/3}/20 = 1.686$ is the overdensity predicted by linear theory at recollapse. In the Monte Carlo method, we ensure that the galaxy collapse redshift is higher than $z = 1$, the redshift at which the cluster is considered to have been assembled (section 3.1), i.e., $z_{\rm coll} > 1$. We solve this equation numerically for $z_{\rm coll}$, and substitute the solution in equation (19), which we then solve to get the radius $s = r_{200}$.

To determine the locations of galaxies inside a cluster, we assume that their distribution is isotropic (in a statistical sense). We can therefore choose the spherical coordinates (θ, ϕ) of each galaxy randomly, using $\phi = 2\pi X_\phi$, and $\cos\theta = 2X_\theta - 1$, where X_ϕ and X_θ are random numbers drawn from a uniform deviate between 0 and 1. We still need to determine the radial co-ordinate r. Using the CNOC cluster survey, Carlberg *et al.* (1997) showed that the radial mass density $\rho(r)$ of matter and the radial number density $\nu(r)$ of galaxies are roughly proportional to each other, where both $\rho(r)$ and $\nu(r)$ are approximated by NFW profiles. Girardi *et al.* (1998) found that the halo mass follows the galaxy distribution in clusters, using a β-model for the halo/galaxy volume density profile. We assume that this proportionality holds for all clusters, and we generalize it to all the density profiles we use. Thus, the assumed background halo mass density profile (equations 3 and 4) gives us $\nu(r)$. We can then select the initial distances r from the cluster center using again a Monte Carlo rejection method. Since the masses and locations of the galaxies have been determined separately, we need to pair them, i.e., for each selected location, to decide which galaxy goes there. We do expect the most massive galaxies to reside near the center of the cluster. However, low-mass galaxies are not all located at large radii, and some of them might be located in the central region of the cluster as well. Indeed, if the galaxies in the central region were all massive, it would be impossible to reproduce the desired number density profile $\nu(r)$ and not have the galaxies overlap.

To prevent any overlap, we locate the galaxies as follows: We first position the most massive galaxy at the center of the cluster. Then we locate the next seven most massive galaxies between radii R_0 and $2R_0$, where R_0 is three times the radius of the most massive galaxy. We then locate the next 19 most massive galaxies between radii $2R_0$ and $3R_0$. Finally, the remaining galaxies are located randomly between radii 0 and $3R_0$. During the process we check that the galaxies do not overlap, by ensuring that the distance between the edges of two galaxies is greater than the radius of the larger galaxy, i.e., $r_{ij} - s_i - s_j > \max(s_i, s_j)$. In the process of locating a galaxy, if this criterion is not satisfied, we simply reject that location and generate a new one.

After assigning the masses, radii, and positions of all the galaxies, we determine the velocity of each galaxy. We consider the velocity a galaxy would have if it were in a perfect circular orbit at radius r,

$$v_{\rm circ}(r) = \left[\frac{G}{r}\left(M_{\rm halo}(r) + \sum_{j,\, r_j < r} m_j\right)\right]^{1/2}\,, \tag{22}$$

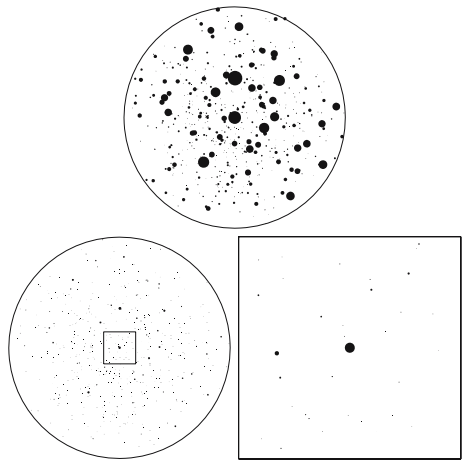

Figure 2. Initial conditions for run A12. Top panel: initial conditions at $z = 1$. The solid circles indicate the virial radii of galaxies. The large circle is the maximum distance $r = 3R_0 = 2.08$ Mpc from the cluster center. Lower left panel: same as top panel, with symbols rescaled to optical diameter of real galaxies. Bottom right panel: enlargement of the central $(0.6\,\mathrm{Mpc})^2$ (box on lower-left panel).

where the sum only includes galaxies inside radius r. The norm of the velocity is chosen by giving a random 10% deviation to the circular velocity, i.e., $v = v_{\mathrm{circ}}(1 + 0.1X_v)$, where X_v is a random number between -1 and 1. For the direction of the velocity, we follow a similar random angle generation technique as we did for the positions of galaxies.

Figure 2 illustrates the initial conditions for one of our simulations (run A12). The top panel shows the cluster at $z = 1$. The large circle represents the maximum distance $3R_0$ within which the galaxies are located initially. Each dot represents a galaxy, with the most massive one located in the center. Even though massive galaxies tend to be larger, there is no direct correspondence between the masses and radii because of the dependence on z_{coll} in equation (19), whose determination involves a Monte Carlo method.

Visually, this looks quite different from the optical pictures of actual clusters like Virgo. This is because each dot has a radius s equal to the virial radius r_{200}, that can exceed the optical radius by an order of magnitude. In the bottom left panel of Fig. 2, we show the same cluster, with all the dots rescaled in size so that the angular diameter of the central galaxy is equal to $8.3'$ at a distance of 16.8 Mpc, which is the observed optical diameter of M87. The bottom right panel shows a zoom-in of the central cluster region. It looks qualitatively similar to pictures of the central region of Virgo.

4. Results

We started by performing 10 series of simulations, for a total of 148 simulations. Table 1 summarizes the characteristics of each series. The first 2 columns show the series name and the number of runs, respectively. The slope of the Schechter luminosity function at $z = 1$ (used to generate the initial conditions) is listed in column 3. Columns 4 to 8 give the characteristics and relevant parameter values of the background cluster halo

Table 1. Series of simulations.

Series (col. 1)	Runs (col. 2)	$\alpha_{\rm start}$ (col. 3)	Profile (col. 4)	β (col. 5)	ρ_0, ρ_s [g cm^{-3}] (col. 6)
A	16	-1.28	β-Virgo	0.33	8.14×10^{-26}
B	17	-1.28	β-Virgo	0.33	8.14×10^{-26}
C	17	-1.36	β-Virgo	0.33	8.14×10^{-26}
D	16	-1.36	β-Virgo	0.33	8.14×10^{-26}
E	16	-1.36	β-Perseus	0.53	7.27×10^{-26}
F	16	-1.36	β-Perseus	0.53	7.27×10^{-26}
G	10	-1.28	NFW	···	2.35×10^{-25}
H	14	-1.31	NFW	···	2.35×10^{-25}
I	10	-1.31	NFW	···	2.35×10^{-25}
J	16	-1.36	β-Perseus	0.53	7.27×10^{-26}

	c (col. 7)	r_c, r_s [kpc] (col. 8)	cD (col. 9)	Harassment (col. 10)	Cluster-growth (col. 11)
A	···	3	×	×	×
B	···	3	×	√	×
C	···	3	×	√	×
D	···	3	√	√	×
E	···	28	×	√	×
F	···	28	√	√	×
G	5	200	×	√	×
H	5	200	×	√	×
I	5	200	√	√	×
J	···	28	×	√	√

profile. Columns 9 and 10 indicate respectively whether a cD galaxy was included in the cluster simulation, and whether galaxy harassment was included as part of the subgrid physics. Column 11 shows if we included cluster mass growth of the simulated cluster.

4.1 *Series A: Initial simulations*

We performed an initial series of 16 simulations, using for the background halo a β-profile with $\beta = 0.33$, a core radius $r_c = 3\,$kpc, and a central density $\rho_0 = 8.14 \times 10^{-26}\,$g cm^{-3}, which is appropriate for a cluster like Virgo (Piffaretti & Kaastra 2006). For this series, we did not include galaxy harassment. Our results are shown in Table 2. It shows the run number (column 1), and at the beginning of the run, the total mass $M_{\rm total}$ in galaxies, in units of $10^{11}\,{\rm M}_\odot$ (column 2), the number of galaxies $N_{\rm total}$ (column 3), and the Schechter luminosity function (equation 18) exponent $\alpha_{\rm start}$ (column 12). This exponent was obtained by performing a numerical fit to the distribution of galaxy masses. Because the masses were determined from a Monte

Table 2. Simulations for series A.

Run	$M_{\rm total}$ [10^{11}M$_\odot$]	$N_{\rm total}$	$N_{\rm merge}$	$N^{\rm gal}_{\rm tides}$	$N_{\rm accr}$	$N^{\rm halo}_{\rm tides}$	$N_{\rm eject}$	$f_{\rm surv}$	f_M	$f_{\rm ICS}$	$\alpha_{\rm start}$	$\alpha_{\rm end}$
A1	855.0	440	137	54	6	0	1	0.550	0.225	0.235	−1.26	−1.23
A2	862.0	702	343	182	24	0	1	0.217	0.490	0.522	−1.28	−1.12
A3	1100.4	480	126	43	7	0	0	0.633	0.136	0.161	−1.28	−1.24
A4	831.0	530	165	67	11	0	0	0.542	0.148	0.161	−1.26	−1.15
A5	980.4	459	175	58	8	0	1	0.473	0.128	0.144	−1.25	−1.18
A6	967.8	640	230	74	5	0	0	0.517	0.157	0.182	−1.29	−1.23
A7	720.0	579	263	114	7	0	0	0.337	0.359	0.384	−1.28	−1.20
A8	757.8	435	200	66	51	0	1	0.269	0.320	0.346	−1.27	−1.26
A9	925.6	514	223	83	12	0	1	0.379	0.245	0.273	−1.28	−1.17
A10	858.9	525	204	54	8	0	0	0.493	0.257	0.260	−1.31	−1.24
A11	880.2	547	224	68	9	0	1	0.448	0.257	0.278	−1.33	−1.25
A12	826.1	548	255	72	15	0	1	0.374	0.225	0.249	−1.29	−1.18
A13	1041.5	431	166	51	6	0	0	0.483	0.275	0.282	−1.27	−1.25
A14	957.3	486	174	52	4	0	0	0.527	0.261	0.265	−1.29	−1.22
A15	860.5	520	160	64	15	0	1	0.538	0.260	0.260	−1.26	−1.18
A16	858.0	483	255	72	8	0	0	0.306	0.323	0.337	−1.28	−1.19

Carlo rejection method, the exponent can differ from the intended value $\alpha = -1.28$ in equation (18) and listed in Table 1, but the deviations are small. Averaging over all runs, we get $\alpha_{\rm start} = -1.280 \pm 0.020$.

Columns 4–8 in Table 2 show the number of galaxies $N_{\rm merge}$ destroyed by mergers, the number of galaxies $N_{\rm tides}^{\rm gal}$ destroyed by tides caused by a massive galaxy, with the fragments dispersed in the ICM, the number of galaxies $N_{\rm accr}$ destroyed by tides caused by a massive galaxy, with the fragments being accreted onto that galaxy, the number of galaxies $N_{\rm tides}^{\rm halo}$ destroyed by the tidal field of the background halo, and the number of galaxies $N_{\rm eject}$ ejected from the cluster, respectively. Column 9 shows the fraction by numbers of galaxies $f_{\rm surv}$ that survive to the present.

We did not find a single occurrence of a galaxy destroyed by tides from the background halo, and the number of galaxies ejected is either 0 or 1. There are large variations in the other numbers from one run to the next, but some trends are apparent. Typically, 50% to 60% of the galaxies are destroyed. Run A2 is an extreme case, with 78% of the galaxies being destroyed. The destruction of galaxies by mergers dominates over the destruction by tides, by more than a factor of 2 except for run A7. If we treat the cases of tidal disruption followed by accretion as being mergers, then mergers dominate even more over tidal disruption. When galaxies are destroyed by tides, the dispersion of fragments into the ICM always dominates over the accretion of fragments onto the massive galaxy, but the ratio varies widely, from 114:7 in run A7 to 66:51 in run A8.

We evaluate the mass fraction $f_{\rm M}$ of galaxies contributing to the intracluster stars,

$$f_{\rm M} = \frac{M_{\rm tides}^{\rm gal} + M_{\rm tides}^{\rm halo}}{M_{\rm total} - M_{\rm eject}}\,, \tag{23}$$

where the letter M refers to the mass in galaxies, rather than their number. The galactic mass contribution to the ICM consists of galaxies destroyed by tides of another more massive galaxy, and by tides of the background halo (though there are no such cases in this series). Column 10 of Table 2 lists the values of $f_{\rm M}$.

We use a mass-dependent mass-to-light ratio of the galaxies having the form (ΛCDM cosmological simulations of Yang *et al.* 2003)

$$\left\langle \frac{M}{L} \right\rangle (M) = \frac{1}{2} \left(\frac{M}{L} \right)_0 \left[\left(\frac{M}{M_1} \right)^{-\gamma_1} + \left(\frac{M}{M_1} \right)^{\gamma_2} \right]. \tag{24}$$

The values of the free parameters are taken as $M_1 = 10^{11.27} h^{-1}{\rm M}_\odot$, $(M/L)_0 = 134\, h{\rm M}_\odot/{\rm L}_\odot$, $\gamma_1 = 0.77$, $\gamma_2 = 0.32$, which are for the best-fitting model of Yang *et al.* (2003) for concordance cosmology. The galaxy masses are converted to luminosities using the mass-to-light ratio. We then calculate the fraction $f_{\rm ICS}$ of the total luminosity of the cluster that comes from intracluster stars,

$$f_{\rm ICS} = \frac{L_{\rm tides}^{\rm gal} + L_{\rm tides}^{\rm halo}}{L_{\rm total} - L_{\rm eject}}\,. \tag{25}$$

The values of $f_{\rm ICS}$ are listed in column 11 of Table 2. Again, there are large variations. In particular, the fraction is very large for run A2, and very small for run A5. Averaging over all runs, we get $f_{\rm ICS} = 0.271 \pm 0.095$. Even though, in most cases about half the

number of galaxies are destroyed, they tend to be low-mass galaxies, which explains why $f_{\rm ICS} < 1 - f_{\rm surv}$, for all the runs.

The galaxies being destroyed by mergers and tides, or escaping are mostly low-mass galaxies. This leads to a flattening of the galaxy mass distribution function. We computed the best numerical fit to the Schechter luminosity function exponent α (equation 18) for the surviving galaxies at the end of the simulations. This is listed as $\alpha_{\rm end}$ in column 13 of Table 2. Averaging over all runs, we get $\alpha_{\rm end} = -1.206 \pm 0.040$.

4.2 *Series B: Turning on harassment*

We modified the algorithm to include the effect of galaxy harassment (see section 2.4.2), and rerun the calculations of series A with the same initial conditions. We also added one more run, B17. The results are shown in Table 3, which follows the same format as Table 2. Comparing with series A, the number of galaxies destroyed by mergers is very similar, but the number of galaxies destroyed by tides tends to be significantly higher. For instance, it goes from 67 to 94 for runs A4–B4, and from 64 to 86 for runs A15–B15. This is because, when a galaxy is subjected to harassment, its binding energy is reduced, and it becomes more prone to experience tidal disruption later. But the number of tidal disruptions followed by accretion does not change significantly. Hence, the additional, tidally-disrupted galaxies almost all contribute to the intracluster stars. The values of $f_{\rm ICS}$ are therefore increased relative to series A. The mean value is $f_{\rm ICS} = 0.288 \pm 0.082$.

This is not significantly larger than for series A. The additional galaxies destroyed are mostly low-mass galaxies. We also recalculated the best-fit Schechter exponent α for the surviving galaxies at $z = 0$. The mean value for the runs in this series is $\alpha_{\rm end} = -1.207 \pm 0.048$.

Figure 3 shows the total galaxy counts in mass bins, obtained by combining all the runs in series B, along with the fitting curves to a Schechter distribution function (equation 18). The best fit Schechter exponent for the initial galaxy distribution (the upper curve at $z = 1$) is $\alpha = -1.28$, and for the final surviving galaxy distribution (the lower curve at $z = 0$) is $\alpha = -1.20$. These values of α were obtained by performing the numerical Schechter function fits on the combined set of galaxies taken from all the 17 runs in this series, which amounts to 8770 initial galaxies at $z = 1$ and 3614 surviving galaxies at $z = 0$.

Clearly from Fig. 3, the fit at $z = 0$ (lower curve) is excellent. This shows that, in our simulations, a Schechter mass (luminosity) distribution function at $z = 1$ remains a Schechter distribution all the way to $z = 0$, though half of the galaxies are destroyed. Only the slope α changes with time.

4.3 *Series C: Steeping up the mass distribution function*

In the simulations of series A and B, the Schechter exponent α evolves from $\alpha \simeq -1.28$ at $z = 1$ to $\alpha \simeq -1.21$ at $z = 0$. Analyzing the combined set of galaxies of all the 17 runs in series B, we obtained the best fit Schechter exponent for the surviving galaxy distribution at $z = 0$ as $\alpha = -1.20$. This is a problem, since the value of $\alpha = -1.28$ is based on observations of nearby clusters (De Propris *et al.* 2003), and should be valid for clusters of galaxies at $z = 0$, whereas we used the same $\alpha = -1.28$ to start our simulations at $z = 1$, and it flattened to $\alpha = -1.20$ at $z = 0$. Ryan *et al.* (2007)

Table 3. Simulations for series B.

Run	$M_{\rm total}$ $[10^{11}{\rm M}_\odot]$	$N_{\rm total}$	$N_{\rm merge}$	$N_{\rm tides}^{\rm gal}$	$N_{\rm accr}$	$N_{\rm tides}^{\rm halo}$	$N_{\rm eject}$	$f_{\rm surv}$	f_M	$f_{\rm ICS}$	$\alpha_{\rm start}$	$\alpha_{\rm end}$
B1	855.0	440	134	62	6	0	1	0.539	0.237	0.248	−1.26	−1.24
B2	862.0	702	337	210	25	0	1	0.184	0.454	0.486	−1.28	−1.11
B3	1100.4	480	126	48	7	0	0	0.623	0.139	0.162	−1.28	−1.24
B4	831.0	530	159	94	12	0	0	0.500	0.184	0.202	−1.26	−1.15
B5	980.4	459	171	78	7	0	1	0.440	0.154	0.175	−1.25	−1.21
B6	967.8	640	226	85	6	0	0	0.505	0.173	0.199	−1.29	−1.23
B7	720.0	579	249	134	9	0	0	0.323	0.364	0.386	−1.28	−1.20
B8	757.8	435	172	79	62	0	1	0.278	0.271	0.293	−1.27	−1.27
B9	925.6	514	223	100	12	0	1	0.346	0.270	0.298	−1.28	−1.19
B10	858.9	525	206	68	7	0	0	0.465	0.298	0.311	−1.31	−1.25
B11	880.2	547	233	85	9	0	1	0.400	0.280	0.301	−1.33	−1.27
B12	826.1	548	241	92	19	0	1	0.356	0.240	0.265	−1.29	−1.20
B13	1041.5	431	160	58	4	0	0	0.485	0.269	0.274	−1.27	−1.26
B14	957.3	486	173	59	5	0	0	0.512	0.274	0.279	−1.29	−1.22
B15	860.5	520	155	86	17	0	1	0.502	0.277	0.278	−1.26	−1.19
B16	858.0	483	264	90	6	0	0	0.255	0.354	0.374	−1.28	−1.16
B17	792.6	451	178	83	16	0	1	0.384	0.346	0.359	−1.24	−1.13

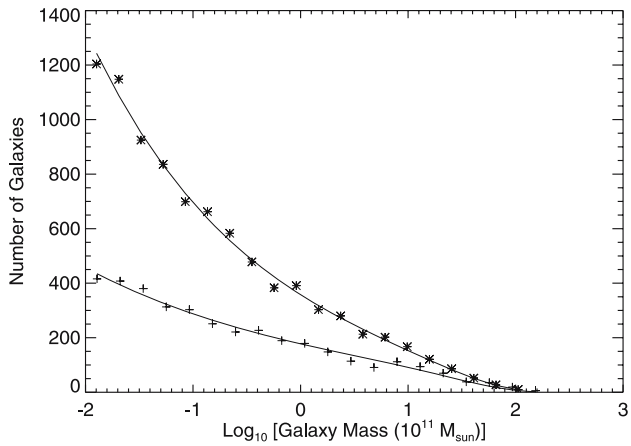

Figure 3. Mass distribution function for galaxies in series B, obtained by adding the numbers for all runs. Results are plotted for initial 8770 galaxies at $z = 1$ (asterisks) and surviving 3614 galaxies at $z = 0$ (plus signs). The curves show the best fit of a Schechter distribution function (equation 18), with $\alpha = -1.28$ at $z = 1$ (upper curve), and $\alpha = -1.20$ at $z = 0$ (lower curve).

recently determined the luminosity function of a large sample of galaxies at $z \simeq 1$, and concluded that there is a steepening of the faint-end slope with redshift, which is expected in the hierarchical formation scenario of galaxies. They obtained a value of the faint-end slope $\alpha = -1.32 \pm 0.07$ at $z = 1$.

In our simulations we take into account this flattening of the luminosity function over time as explained. The results of series A and B suggest that $|\alpha|$ decreases by ~ 0.08 between $z = 1$ and $z = 0$. Using this as a guide, we performed a new series of simulations, series C, using $\alpha_{\rm start} = -1.36$, with the hope that this value will evolve toward something close to $\alpha = -1.28$ at $z = 0$. The results are shown in Table 4. The average values of α are $\alpha_{\rm start} = -1.357 \pm 0.021$ and $\alpha_{\rm end} = -1.272 \pm 0.050$.

A plot analogous to Fig. 3 showed that at $z = 0$, a Schechter distribution function is still a good approximation to the mass distribution. The value of $\alpha_{\rm end}$ is close enough to our target value of -1.28. So from now on, in all subsequent series with the β model halo density profile, we will use an initial α of -1.36, as shown in Table 1. This value is well inside the range obtained by Ryan *et al.* (2007).

Using a steeper galaxy distribution while still requiring that the clusters contain 25 galaxies with $L > 0.2L_*$ (initial conditions in section 3.2) results in the initial number of galaxies being larger by a factor of about 2 (column 3 of Table 4). But the numbers of galaxies destroyed by mergers and tides are also higher relative to series B. As a result the trends are similar. In particular, mergers still dominate over tides by more than a factor of 2.

The run C1 has a larger number of galaxies ejected from the cluster. This is because the most massive galaxy, located at the center of the cluster, was particularly large. Its radius was $s = 385$ kpc, compared to $s < 300$ kpc for the other runs. This increased the value of R_0 (see section 3.2) used for setting up the initial conditions. As a result, more galaxies were located at larger radii, where they are more likely to escape. The mean value of $f_{\rm ICS}$ for this series is $f_{\rm ICS} = 0.302 \pm 0.088$.

Table 4. Simulations for series C.

Run	$M_{\rm total}$ $[10^{11}{\rm M}_\odot]$	$N_{\rm total}$	$N_{\rm merge}$	$N_{\rm tides}^{\rm gal}$	$N_{\rm accr}$	$N_{\rm tides}^{\rm halo}$	$N_{\rm eject}$	$f_{\rm surv}$	f_M	$f_{\rm ICS}$	$\alpha_{\rm start}$	$\alpha_{\rm end}$
C1	1144.3	948	322	123	13	0	7	0.509	0.162	0.179	−1.34	−1.27
C2	1009.9	936	283	138	19	0	1	0.529	0.195	0.218	−1.38	−1.30
C3	914.2	603	316	97	13	0	0	0.294	0.265	0.297	−1.35	−1.24
C4	970.5	635	162	86	11	0	1	0.591	0.216	0.227	−1.32	−1.28
C5	935.9	672	250	101	7	0	1	0.466	0.158	0.175	−1.33	−1.25
C6	948.2	1136	502	268	6	0	0	0.317	0.318	0.337	−1.35	−1.21
C7	926.4	884	276	155	10	0	1	0.500	0.258	0.270	−1.35	−1.28
C8	818.4	696	347	142	62	0	1	0.207	0.423	0.443	−1.35	−1.26
C9	875.9	903	421	255	44	0	1	0.202	0.405	0.416	−1.34	−1.19
C10	1110.5	785	286	100	20	0	1	0.482	0.168	0.190	−1.39	−1.39
C11	864.2	809	338	139	18	0	1	0.387	0.386	0.405	−1.40	−1.36
C12	1053.2	978	395	212	29	0	0	0.350	0.294	0.303	−1.36	−1.29
C13	1151.7	790	344	127	24	0	1	0.372	0.262	0.282	−1.37	−1.29
C14	876.8	684	335	133	23	0	1	0.281	0.320	0.341	−1.37	−1.21
C15	788.0	769	240	140	27	0	0	0.471	0.243	0.263	−1.35	−1.26
C16	905.1	578	284	80	24	0	1	0.327	0.430	0.434	−1.36	−1.29
C17	889.2	822	325	169	13	0	0	0.383	0.323	0.347	−1.36	−1.25

4.4 *Series D: Adding a cD galaxy*

A cD (*central dominant*) galaxy is a very bright supergiant elliptical galaxy with an extended envelope (or a *diffuse* halo) found at the center of a cluster (Schombert 1988). Several galaxy clusters have been found to have cD galaxies at their centers (e.g., Quintana & Lawrie 1982; Oegerle & Hill 2001; Jordan *et al.* 2004). We performed some simulations by incorporating a cD galaxy in the clusters. Being the brightest and most massive cluster galaxy, the mass of a cD is larger than the prediction of the normal Schechter distribution function (equation 18). So we introduced the cD galaxy manually at our simulated cluster center. We adopted a luminosity of $L_{\rm cD} = 10L^*$, which is a canonical value for a cD. Using a constant mass to light ratio ($\Upsilon = 193\,{\rm h}\,{\rm M}_\odot/{\rm L}_\odot$, section 3.2), this corresponds to a cD galaxy mass of $M_{\rm cD} = 437.6 \times 10^{11}{\rm M}_\odot$. When we wanted a cD galaxy present in the simulation we changed the mass of the cluster central galaxy (see sectoin 3.2) to the cD mass, $M_{\rm cD}$. This allowed us to keep the appropriate initial galaxy distribution for a cluster while incorporating a cD galaxy at rest, located at the center.

We performed simulations by adding a cD galaxy to our Virgo-like cluster, and called it series D. The results are listed in Table 5, from which certain trends are clear after incorporating a cD galaxy in the simulation. The total galaxy mass increases since a massive cD galaxy is being added. More prominent than in the previous series A, B, and C, here galaxy mergers outnumber tides by factors $\sim$ 2–3, which go as high as 4 in run D12.

A striking new feature in cases incorporating a cD galaxy is the increase in the number of accretions after tidal disruption by a galaxy, fully 1/4 of the galaxies being acreted in run D5. Since in these accretions, the smaller galaxy is tidally destroyed and is absorbed (or merged) by the massive galaxy (section 2.4.4), it appears, in our simulated clusters, that in the presence of a cD galaxy the number of effective mergers is very high.

The luminosity fraction imparted to ICS has decreased in all the runs, with a value as low as 0.085 in run D6. To explain such a result, we note that the most massive central galaxy (cD or otherwise) in our simulated cluster is never destroyed because of its large mass. In an encounter, it is normally the lower-mass galaxy that gets destroyed. Also the initial conditions of the most massive galaxy (at rest at the center, see section 3.2) make it less likely to be destroyed by the tidal field of the halo. If the central galaxy is a cD, a large mass fraction (as high as 38% in run D11) is locked into it, which can never contribute to the ICS. So a smaller mass fraction is available to be transferred to the ICS, which eventually leads to a decrease in $f_{\rm ICS}$. The mean value of $f_{\rm ICS}$ for series D is $f_{\rm ICS} = 0.161 \pm 0.047$.

4.5 *Series E & F: Other β profiles*

In the next two series of runs, we consider a different background halo. We use a β-profile with $\beta = 0.53$, a core radius $r_c = 28\,{\rm kpc}$ and a central density $\rho_0 = 7.27 \times 10^{-26}\,{\rm g\,cm^{-3}}$, which is appropriate for a cluster like Perseus (Piffaretti & Kaastra 2006). Series E and F do not include, and include a cD galaxy, respectively (hence series E should be compared with series C, and series F with series D).

The results for series E are shown in Table 6. The most notable feature is that some galaxies are destroyed by the tidal field of the background halo, something

Table 5. Simulations for series D.

Run	$M_{\rm total}$ [$10^{11}{\rm M}_\odot$]	$N_{\rm total}$	$N_{\rm merge}$	$N_{\rm tides}^{\rm gal}$	$N_{\rm accr}$	$N_{\rm tides}^{\rm halo}$	$N_{\rm eject}$	$f_{\rm surv}$	f_M	$f_{\rm ICS}$	$\alpha_{\rm start}$	$\alpha_{\rm end}$
D1	1394.6	1023	345	165	83	0	0	0.420	0.127	0.160	−1.38	−1.33
D2	1374.4	866	330	97	37	0	1	0.463	0.085	0.113	−1.38	−1.33
D3	1431.1	906	257	199	187	0	0	0.290	0.125	0.156	−1.39	−1.32
D4	1163.2	754	211	152	120	0	0	0.359	0.117	0.156	−1.33	−1.26
D5	1239.5	788	283	167	197	0	0	0.179	0.167	0.213	−1.33	−1.21
D6	1158.8	527	131	59	53	0	1	0.537	0.065	0.085	−1.34	−1.30
D7	1300.7	663	236	85	73	0	1	0.404	0.151	0.204	−1.37	−1.31
D8	1298.4	773	296	113	116	0	0	0.321	0.120	0.159	−1.36	−1.33
D9	1299.5	652	256	95	63	0	1	0.364	0.141	0.186	−1.39	−1.33
D10	1169.4	589	193	76	67	0	1	0.428	0.106	0.143	−1.37	−1.32
D11	1145.8	741	282	143	79	0	1	0.318	0.124	0.157	−1.38	−1.25
D12	1227.5	732	235	57	22	0	9	0.559	0.075	0.099	−1.39	−1.35
D13	1334.2	952	330	166	70	0	0	0.406	0.151	0.199	−1.35	−1.31
D14	1286.0	844	283	184	115	0	1	0.309	0.203	0.266	−1.34	−1.24
D15	1470.8	888	298	115	56	0	0	0.472	0.140	0.173	−1.36	−1.33
D16	1454.4	966	288	170	125	0	0	0.396	0.086	0.109	−1.34	−1.30

Table 6. Simulations for series E.

Run	$M_{\rm total}$ [10^{11}M$_\odot$]	$N_{\rm total}$	$N_{\rm merge}$	$N_{\rm tides}^{\rm gal}$	$N_{\rm accr}$	$N_{\rm tides}^{\rm halo}$	$N_{\rm eject}$	$f_{\rm surv}$	f_M	$f_{\rm ICS}$	$\alpha_{\rm start}$	$\alpha_{\rm end}$
E1	1065.4	1023	406	159	24	8	1	0.415	0.297	0.313	−1.38	−1.31
E2	1034.0	866	326	104	7	6	2	0.486	0.168	0.192	−1.38	−1.31
E3	1051.3	906	405	213	19	14	0	0.282	0.446	0.464	−1.38	−1.27
E4	799.4	754	250	177	35	7	0	0.378	0.391	0.424	−1.34	−1.25
E5	868.7	788	394	201	42	12	0	0.176	0.492	0.521	−1.32	−1.22
E6	795.8	527	154	67	7	6	1	0.554	0.303	0.314	−1.34	−1.29
E7	947.7	663	276	97	9	3	1	0.418	0.376	0.398	−1.37	−1.31
E8	941.0	773	395	121	11	8	0	0.307	0.348	0.381	−1.37	−1.28
E9	934.5	652	263	109	10	6	1	0.403	0.325	0.350	−1.39	−1.34
E10	807.5	589	210	98	11	5	1	0.325	0.448	0.343	−1.38	−1.35
E11	760.7	741	349	142	9	8	1	0.313	0.283	0.314	−1.48	−1.23
E12	946.4	732	227	57	4	2	28	0.566	0.149	0.178	−1.39	−1.35
E13	953.4	952	344	180	14	11	0	0.423	0.349	0.377	−1.35	−1.29
E14	950.5	844	325	197	23	6	1	0.346	0.395	0.435	−1.33	−1.29
E15	1145.5	888	320	118	13	5	0	0.486	0.339	0.342	−1.36	−1.29
E16	1125.4	966	439	146	10	10	1	0.373	0.393	0.422	−1.34	−1.26

that never happened with Virgo-like clusters. In order to explain such a behavior we note that tidal disruption by the cluster halo generally occurs with galaxies at a distance $r < 1$ Mpc from the cluster center. Our simulated Perseus-like cluster halo mass profile rises more steeply than the Virgo-like cluster up to $\sim$1.7 Mpc, making Perseus more massive in the inner regions. So a galaxy at a smaller distance, precisely at $r < 1.7$ Mpc, from the cluster center feels a larger tidal field from a more massive halo, and is more prone to be disrupted in the Perseus-like cluster.

The numbers of other galaxy outcomes are comparable for Perseus-like and Virgo-like clusters, with mergers dominating over tides. The mean $f_{\rm ICS}$ for series E is $f_{\rm ICS} = 0.360 \pm 0.090$. This $f_{\rm ICS}$ is somewhat larger than the Virgo-like cluster mean (series C). This can be attributed to the non-zero tidal disruption by the cluster halo, resulting here in a finite contribution to the ICS luminosity fraction.

Table 7 shows the results for series F, i.e., simulations of a Perseus-like cluster with a cD galaxy at the center. Here few galaxies are destroyed by the tidal field of the cluster halo, yet the number is smaller than in series E. It appears, then that the presence of a cD galaxy reduces the number of tidal disruptions by the background halo, since galaxies that would be destroyed by the tidal field of the central parts of the halo are being destroyed by the cD galaxy instead.

Comparing the results for series D and series F (Virgo-like and Perseus-like clusters with a cD galaxy,) the numbers – merger, galaxy-tide and accretion are similar. Series F continues the trend of increased accretions when a cD galaxy is introduced. Also series F has a smaller fraction of luminosity going to ICS. The mean $f_{\rm ICS}$ for series F is $f_{\rm ICS} = 0.166 \pm 0.041$. This $f_{\rm ICS}$ is very similar to that of the relevant Virgo-like cluster mean (series D). This implies that in the presence of a cD galaxy, the ICS luminosity fraction is not so sensitive to the parameters of the β-model density profile.

4.6 *Series G, H & I: NFW profile*

We now consider a background halo described by a NFW profile (see section 2.3, equation 4), with a scale radius $r_s = 200$ kpc, and a concentration parameter $c = 5$. These values are adopted from observational studies of galaxy clusters (Arabadjis *et al.* 2002; Pratt & Arnaud 2005; Maughan *et al.* 2007) where the authors found the best fitting NFW model parameters for cluster mass profiles.

We do not necessarily expect the flattening of the Schechter mass function to be the same for the NFW profile halo and the β-profile halo. So at first we performed a series with $\alpha = -1.28$ (see Table 1), and called it series G. The results are listed in Table 8.

To contrast an NFW-model cluster with a β-model cluster, series G should be compared with series B, since these are with $\alpha = -1.28$, include galaxy harassment, and no cD galaxy. The most striking feature is the large number of galaxies destroyed by the tidal field of the NFW cluster halo. This halo tidal disruption was nil (in the Virgo-like cluster) to a handful (in the Perseus-like cluster) for the β-model background halo. With the NFW profile, the number of halo tides is comparable to the galaxy tides, even exceeding the latter in runs G5 and G6.

The reason for such a behavior is that the NFW halo mass profile rises much more steeply than the β-model mass profile of a Virgo-like cluster up to a distance $r \sim 1.9$ Mpc. So the NFW halo is significantly more massive (by factors as high as 4–5) than the β-model halo at distances $r < 1$ Mpc, where halo tides are dominant

Table 7. Simulations for series F.

Run	$M_{\rm total}$ [10^{11}M$_\odot$]	$N_{\rm total}$	$N_{\rm merge}$	$N^{\rm gal}_{\rm tides}$	$N_{\rm accr}$	$N^{\rm halo}_{\rm tides}$	$N_{\rm eject}$	$f_{\rm surv}$	f_M	$f_{\rm ICS}$	$\alpha_{\rm start}$	$\alpha_{\rm end}$
F1	1394.6	1023	386	153	88	4	1	0.382	0.138	0.174	−1.38	−1.28
F2	1374.4	866	304	96	47	1	2	0.480	0.106	0.136	−1.38	−1.33
F3	1431.1	906	277	183	196	1	0	0.275	0.144	0.185	−1.39	−1.25
F4	1163.2	754	211	180	109	0	0	0.337	0.126	0.165	−1.33	−1.27
F5	1239.5	788	288	166	199	0	0	0.171	0.158	0.202	−1.33	−1.21
F6	1158.8	527	141	60	55	1	1	0.510	0.092	0.115	−1.34	−1.29
F7	1300.7	663	253	81	70	1	1	0.388	0.113	0.155	−1.37	−1.28
F8	1298.4	773	295	124	108	2	0	0.316	0.134	0.173	−1.36	−1.29
F9	1299.5	652	226	93	61	2	1	0.413	0.153	0.202	−1.39	−1.38
F10	1169.4	589	182	83	72	0	1	0.426	0.133	0.178	−1.37	−1.33
F11	1145.8	741	269	148	76	1	1	0.332	0.154	0.201	−1.38	−1.29
F12	1227.5	732	194	58	26	0	31	0.578	0.067	0.090	−1.39	−1.36
F13	1334.1	952	322	175	85	1	0	0.388	0.121	0.154	−1.35	−1.29
F14	1286.0	844	272	180	107	0	1	0.336	0.197	0.259	−1.34	−1.30
F15	1470.8	888	306	103	54	1	0	0.478	0.108	0.134	−1.36	−1.31
F16	1454.4	966	314	155	135	2	1	0.372	0.097	0.126	−1.34	−1.29

Table 8. Simulations for series G.

Run (col. 1)	$M_{\rm total}$ [10^{11}M$_\odot$] (col. 2)	$N_{\rm total}$ (col. 3)	$N_{\rm merge}$ (col. 4)	$N_{\rm tides}^{\rm gal}$ (col. 5)	$N_{\rm accr}$ (col. 6)	$N_{\rm tides}^{\rm halo}$ (col. 7)
G1	721.9	372	72	55	6	47
G2	1034.3	637	129	80	4	63
G3	821.1	530	127	89	5	73
G4	992.3	457	113	61	9	44
G5	899.7	618	94	56	7	64
G6	947.1	452	95	31	2	34
G7	865.2	542	170	91	7	77
G8	1011.6	725	169	101	7	71
G9	1100.6	726	214	144	17	103
G10	1174.4	619	190	76	2	57
	$N_{\rm eject}$ (col. 8)	$f_{\rm surv}$ (col. 9)	f_M (col. 10)	$f_{\rm ICS}$ (col. 11)	$\alpha_{\rm start}$ (col. 12)	$\alpha_{\rm end}$ (col. 13)
G1	1	0.513	0.486	0.498	−1.27	−1.26
G2	7	0.556	0.405	0.406	−1.29	−1.26
G3	1	0.443	0.587	0.589	−1.31	−1.29
G4	1	0.501	0.211	0.229	−1.28	−1.26
G5	8	0.629	0.443	0.443	−1.29	−1.28
G6	17	0.604	0.263	0.288	−1.31	−1.32
G7	1	0.362	0.543	0.555	−1.31	−1.25
G8	1	0.519	0.502	0.510	−1.24	−1.20
G9	1	0.340	0.467	0.501	−1.27	−1.23
G10	6	0.465	0.458	0.454	−1.28	−1.23

(as discussed in section 4.5). Consequently galaxies near the cluster center experience a larger tidal field and are more likely to be tidally disrupted.

This larger number of halo tides alters several results in our simulated NFW model cluster as compared to the β-model. The mergers exceed the galaxy tides, usually by factors 1.3–1.8 (except runs G6 and G10, where the factors are 3 and 2.5). But when tides by galaxy and cluster halo are added together, they become comparable to or even exceed the number of mergers. The accretions are always small in number, and when added to mergers do not have much effect on the above.

The mean $f_{\rm ICS}$ for series G is $f_{\rm ICS} = 0.447 \pm 0.113$. This is significantly larger than the ICS luminosity fraction obtained with the β-model clusters. The reason is again the numerous halo tides. Some massive galaxies are being destroyed by the tidal field of the NFW halo, when they come near the cluster center, and this is contributing a large mass (and luminosity) fraction to the ICS. In this series G, we obtained the average values of α as $\alpha_{\rm start} = -1.285 \pm 0.022$ and $\alpha_{\rm end} = -1.258 \pm 0.034$.

Also combining the set of galaxies of all the 10 runs in series G, we obtained the best fit Schechter exponent for the surviving galaxy distribution at $z = 0$ as $\alpha = -1.25$. Analogous to our approach for the β-model in section 4.3, we note that $|\alpha|$ decreases by $\sim$0.03 between $z = 1$ and $z = 0$. So we performed a new series of simulations,

series H, using $\alpha_{\rm start} = -1.31$, expecting that this will evolve to $\alpha \sim -1.28$ at $z = 0$. This series includes galaxy harassment but no cD galaxy. The results for series H are shown in Table 9.

Series H continues the trends of series G pertaining to a NFW profile. There are a large number of halo tides that dominate the mass fraction, and result in a high value of $f_{\rm ICS}$. The combined numbers of tidal disruptions (by galaxy and halo) are comparable to or exceed the numbers of mergers. The mean $f_{\rm ICS}$ for series H is $f_{\rm ICS} = 0.491 \pm 0.132$. In this series H, we obtained the average values of α as $\alpha_{\rm start} = -1.310 \pm 0.020$ and $\alpha_{\rm end} = -1.288 \pm 0.036$.

We then performed a series of simulations by putting a cD galaxy at the center of the NFW cluster halo, and called it series I. The results are shown in Table 10. Here, the numbers of tides by the cluster halo and by other galaxies are comparable; when added the total occurrence of tides compares to or exceeds that of mergers. Comparing series H and series I (NFW-type clusters respectively without and with a cD galaxy,) there are more accretions when a cD galaxy is introduced (similar to series D and F). The trend seen before with the Perseus-like clusters (between series E and F), that the number of tidal disruptions by the background halo reduces in the presence of a cD galaxy, is almost absent in the NFW-type clusters. Galaxies approaching the cluster center get destroyed by the tidal field of the halo before the cD galaxy can have any effect.

The galactic luminosity fractions dispersed into the ICM are neither too high, nor too low. We suspect this is the combined effect of putting a cD galaxy in an NFW type cluster. There is a tendency of the ICS luminosity fraction to be high in an NFW model cluster, and a cD galaxy tends to reduce the luminosity fraction imparted to the ICM. These two opposing trends cause the $f_{\rm ICS}$ values to be moderate in series I. Here the mean $f_{\rm ICS}$ is $f_{\rm ICS} = 0.381 \pm 0.059$.

4.7 *Series J: Cluster mass growth*

We performed a series of simulation in which we consider mass growth of the background cluster halo with time by accretion. The mass growth rate is adopted from the N-body simulations of Wechsler *et al.* (2002), where the functional fit to the mass accretion histories of dark matter halos is given by

$$M(z) = M_0 e^{-\kappa z}. \tag{26}$$

Here, $M(z)$ is the halo mass at $z > 0$, M_0 is the final halo mass at $z = 0$, and κ is a constant depending on halo mass. Figure 4 of Wechsler *et al.* (2002) plots the average mass accretion histories, from which we read $M(z = 1)/M_0 \sim 0.75$ for massive halos ($M_0 > 3 \times 10^{13} {\rm h}^{-1} {\rm M}_\odot$). Hence we consider that there has been 33% growth of halo mass from $z = 1$ to $z = 0$, the evolution time in our simulations (section 3.1).

We assume that the density profile of the cluster halo remains the same. We calculate the initial halo mass at $z = 1$ using a β-profile with $\beta = 0.53$, a core radius $r_c = 28$ kpc and a central density $\rho_0 = 7.27 \times 10^{-26}$ g cm^{-3}, which is appropriate for the Perseus cluster (section 4.5). This halo is then allowed to evolve up to $z = 0$ according to the mass growth rate in equation (26). We use, for each run, exactly the same initial conditions as in series E.

The results for series J are shown in Table 11. Comparing series E and series J (Perseus type clusters respectively without and with cluster growth), there are more

Table 9. Simulations for series H.

Run	$M_{\rm total}$ $[10^{11}{\rm M}_\odot]$	$N_{\rm total}$	$N_{\rm merge}$	$N_{\rm tides}^{\rm gal}$	$N_{\rm accr}$	$N_{\rm tides}^{\rm halo}$	$N_{\rm eject}$	$f_{\rm surv}$	f_M	$f_{\rm ICS}$	$\alpha_{\rm start}$	$\alpha_{\rm end}$
H1	894.3	755	171	152	5	122	0	0.404	0.620	0.656	−1.33	−1.33
H2	866.2	556	195	68	5	92	1	0.351	0.563	0.596	−1.28	−1.24
H3	955.0	621	161	84	2	67	1	0.493	0.396	0.394	−1.33	−1.35
H4	758.6	588	153	113	7	109	1	0.349	0.702	0.724	−1.30	−1.30
H5	1103.6	997	197	132	5	68	22	0.575	0.375	0.407	−1.30	−1.26
H6	1008.7	774	266	162	10	148	0	0.243	0.682	0.704	−1.29	−1.24
H7	1027.4	639	101	40	4	47	28	0.656	0.316	0.342	−1.32	−1.30
H8	833.8	601	126	75	5	70	7	0.529	0.496	0.498	−1.29	−1.28
H9	740.3	494	109	53	9	54	4	0.536	0.398	0.417	−1.30	−1.28
H10	952.9	744	159	96	13	92	1	0.515	0.451	0.474	−1.35	−1.32
H11	779.4	519	113	54	9	59	2	0.543	0.375	0.391	−1.31	−1.25
H12	993.6	741	163	86	3	57	10	0.570	0.306	0.320	−1.33	−1.29
H13	931.8	534	131	60	5	62	2	0.513	0.412	0.423	−1.31	−1.33
H14	1012.8	748	202	117	8	95	1	0.434	0.508	0.534	−1.30	−1.26

Table 10. Simulations for series I.

Run (col. 1)	$M_{\rm total}$ $[10^{11}{\rm M}_{\odot}]$ (col. 2)	$N_{\rm total}$ (col. 3)	$N_{\rm merge}$ (col. 4)	$N_{\rm tides}^{\rm gal}$ (col. 5)	$N_{\rm accr}$ (col. 6)	$N_{\rm tides}^{\rm halo}$ (col. 7)
I1	1189.1	495	114	53	26	75
I2	1255.5	705	183	100	16	87
I3	1189.9	643	152	127	35	119
I4	1153.5	548	108	78	8	66
I5	1309.4	821	228	139	19	87
I6	1330.8	596	105	56	2	54
I7	1315.8	775	215	126	37	105
I8	1188.1	691	118	91	12	71
I9	1236.6	574	103	73	12	56
I10	1093.4	634	96	96	8	64
	$N_{\rm eject}$ (col. 8)	$f_{\rm surv}$ (col. 9)	f_M (col. 10)	$f_{\rm ICS}$ (col. 11)	$\alpha_{\rm start}$ (col. 12)	$\alpha_{\rm end}$ (col. 13)
I1	1	0.457	0.322	0.399	−1.34	−1.31
I2	0	0.452	0.326	0.423	−1.34	−1.32
I3	0	0.327	0.391	0.494	−1.29	−1.31
I4	1	0.524	0.255	0.335	−1.32	−1.30
I5	1	0.423	0.341	0.445	−1.33	−1.31
I6	9	0.621	0.265	0.334	−1.31	−1.30
I7	0	0.377	0.299	0.372	−1.33	−1.31
I8	1	0.576	0.248	0.305	−1.36	−1.35
I9	1	0.573	0.295	0.344	−1.32	−1.30
I10	1	0.582	0.274	0.359	−1.31	−1.29

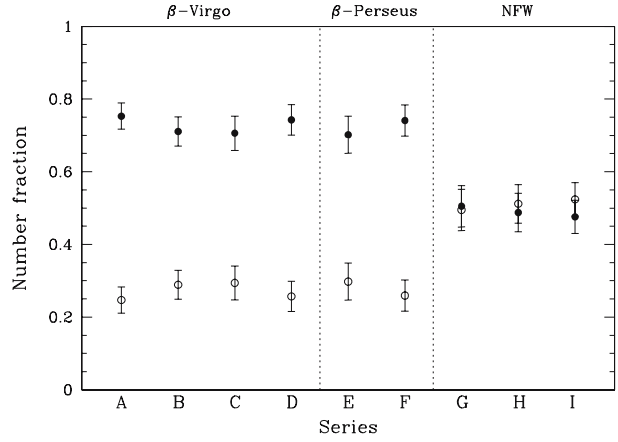

Figure 4. Fractional number of galaxies destroyed by mergers, $f_{\rm destroyed}^{\rm mergers}$ (filled circles), and by tides, $f_{\rm destroyed}^{\rm tides}$ (open circles), averaged over all runs within each series of Table 1. Error bars show the standard deviation.

Table 11. Simulations for series J.

Run	$M_{\rm total}$ $[10^{11}{\rm M}_\odot]$	$N_{\rm total}$	$N_{\rm merge}$	$N_{\rm tides}^{\rm gal}$	$N_{\rm accr}$	$N_{\rm tides}^{\rm halo}$	$N_{\rm eject}$	$f_{\rm surv}$	f_M	$f_{\rm ICS}$	$\alpha_{\rm start}$	$\alpha_{\rm end}$
J1	1065.4	1023	462	194	24	9	1	0.326	0.308	0.324	−1.38	−1.25
J2	1034.0	866	350	114	10	10	1	0.440	0.316	0.342	−1.38	−1.34
J3	1051.3	906	430	233	22	16	0	0.226	0.474	0.496	−1.38	−1.25
J4	799.4	754	263	193	29	12	0	0.341	0.508	0.523	−1.34	−1.25
J5	868.7	788	402	220	43	13	0	0.140	0.570	0.598	−1.32	−1.24
J6	795.8	527	167	81	10	13	1	0.484	0.404	0.425	−1.34	−1.28
J7	947.7	663	278	119	10	4	1	0.379	0.451	0.473	−1.37	−1.31
J8	941.0	773	412	132	9	8	0	0.274	0.400	0.436	−1.37	−1.26
J9	934.5	652	303	105	10	8	1	0.345	0.374	0.404	−1.39	−1.29
J10	807.5	589	239	100	13	4	1	0.394	0.355	0.379	−1.38	−1.32
J11	760.7	741	362	157	7	10	1	0.275	0.416	0.445	−1.38	−1.24
J12	946.4	732	274	55	4	6	9	0.525	0.233	0.275	−1.39	−1.34
J13	953.4	952	389	201	14	15	0	0.350	0.388	0.422	−1.35	−1.26
J14	950.5	844	329	227	27	8	1	0.299	0.462	0.493	−1.33	−1.28
J15	1145.5	888	366	142	17	7	0	0.401	0.340	0.345	−1.36	−1.28
J16	1125.4	966	459	161	12	13	1	0.331	0.476	0.478	−1.34	−1.27

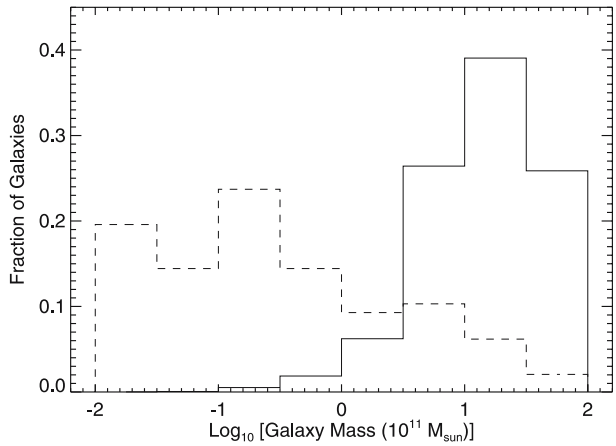

Figure 5. Mass histogram of number fraction (*dashed line*) and luminosity fraction (*solid line*) of galaxies contributing to the ICL in run C3.

galaxy interactions in the growing cluster, which cause the survival fraction to decrease. In series J, the numbers of mergers and galaxy tidal disruptions increase by factors up to 1.2. The numbers of accretions, halo tides, and ejections remain almost same or increase slightly.

There is an increase in the ICS luminosity fraction in the growing cluster, because of the larger number of tidal disruptions. The mean $f_{\rm ICS}$ in series J is $f_{\rm ICS} = 0.429 \pm 0.083$. This is somewhat higher than the mean value in series E.

5. Discussion

5.1 *Mergers and tides*

To quantify the relative importance of destruction by tides and by mergers, we calculated, for each run, the following fractional numbers:

$$f_{\rm destroyed}^{\rm mergers} = \frac{N_{\rm merge} + N_{\rm accr}}{N_{\rm destroyed}}, \tag{27}$$

$$f_{\rm destroyed}^{\rm tides} = \frac{N_{\rm tides}^{\rm gal} + N_{\rm tides}^{\rm halo}}{N_{\rm destroyed}}, \tag{28}$$

where $N_{\rm destroyed} = N_{\rm merge} + N_{\rm tides}^{\rm gal} + N_{\rm accr} + N_{\rm tides}^{\rm halo}$. We then averaged the fractions over all the runs in each series of the simulations. The results for the set of series in Table 1 are shown in Fig. 4. The destruction by mergers clearly dominates over destruction by tides for the β model, while they are of comparable importance for the NFW model.

In order to investigate the mass distribution of the galaxies contributing to the ICL in our simulations, we plotted the mass histograms of the number fractions and the luminosity fractions of such galaxies in run C3, as shown in Fig. 5. These fractions are with respect to all the galaxies ending up in the ICM in this run. While most of

the galaxies destroyed by tides are dwarfs, the destruction of few galaxies of mass $M > 10^{11}\mathrm{M}_{\odot}$ provides more than 60% of the intracluster light.

We can show that, contrary to popular belief, the destruction of DGs alone cannot explain the observed ICL. We calculated the total light fraction of all the galaxies (destroyed or not) with $M < 10^{11}\mathrm{M}_{\odot}$ in our simulated cluster of run C3. This would be the fraction of intracluster light if all DGs, and only DGs, were destroyed. We get the luminosity fraction of DGs as 0.034, which is smaller than the most observed ICL fraction values. To obtain larger values, compatible with observations, either (1) clusters must contain dwarfs many times more than a Schechter distribution would predict, (2) dwarfs galaxies have a much lower M/L ratio than we assumed, or (3) some intermediate-mass or massive galaxies are destroyed.

The last argument is the most plausable, and it is supported by our simulations: some intermediate-mass or massive galaxies are getting destroyed by the tidal field of the most massive galaxy. Note that in this high mass range we are in the exponential tail of the Schechter distribution. The mass ratios between the most massive galaxy and the high-mass ones destroyed are factors of about 3 to 5, so destruction by tides is viable.

5.2 *Intracluster stars*

There have been several observational measurements of the light fraction contained in the ICS with respect to the total light in a cluster. We collected some values of the ICS fraction from the literature, and list them in Table 12. In Fig. 6 we show the ICS luminosity fraction we obtained in our simulations, plotted as horizontal lines showing the average f_{ICS} from the runs in series A–J (Table 1, section 4). For comparison, the observed f_{ICS} values (from Table 12) are shown by the symbols and error bars. We can clearly see that the ICS luminosity fraction in clusters from observations fall well within our simulation predictions. A few clusters have too small f_{ICS}, which are probably galaxy groups and low-mass clusters.

Our simulation results indicate that the tidal destruction of galaxies (by other galaxies and by the cluster halo) in clusters can sufficiently explain the observed fraction of ICL. Also our results (in section 4) imply that for each cluster halo density profile, namely, β and NFW models, f_{ICS} increases with the mass of the cluster halo. This is consistent with the studies finding that more massive clusters have a larger fraction of ICL than the less massive ones (Lin & Mohr 2004; Murante *et al.* 2004).

5.3 *Limitations of the method*

The strengths and weaknesses of the methodology used in this work both reside in our somehow original approach of using one single particle to represent each galaxy, combined with a subgrid treatment of galaxy mergers, tidal disruption, and galaxy harassment.

On the positive side, this approach has enabled us to perform a very large number of simulations (148 total), covering a fairly large parameter space, while obtaining statistically significant results. Doing this many simulations without resorting to subgrid physics would have been computationally prohibitive. In implementing the subgrid physics, we have attempted to make the most reasonable choices possible.

Table 12. Observed values of the intracluster light fraction.

Index	Cluster	$f_{\rm ICS}$ (%)	$\Delta f_{\rm ICS}$ (%)	Reference
1.	Coma	50	–	Bernstein *et al.* (1995)
2.	Abell 1689	30	–	Tyson & Fischer (1995)
3.	Abell 1651	<5	–	Gonzalez *et al.* (2000)
4.	M96 (Leo) group	<1.6	–	Castro-Rodriguez *et al.* (2003)
5.	HCG 90	45	5	White *et al.* (2003)
6.	Virgo	15.8	8	Feldmeier *et al.* (2004b)
7.	A801	16	4.7	Feldmeier *et al.* (2004a)
8.	A1234	17	4.4	Feldmeier *et al.* (2004a)
9.	A1553	21	16	Feldmeier *et al.* (2004a)
10.	A1914	28	16	Feldmeier *et al.* (2004a)
11.	93 clusters	50	10	Lin & Mohr (2004)
12.	683 clusters	10.9	5.0	Zibetti *et al.* (2005)
13.	A4059	22	12	Krick & Bernstein (2007)[a]
14.	A3880	14	6	Krick & Bernstein (2007)
15.	A2734	19	6	Krick & Bernstein (2007)
16.	A2556	6	5	Krick & Bernstein (2007)
17.	A4010	21	8	Krick & Bernstein (2007)
18.	A3888	13	5	Krick & Bernstein (2007)
19.	A3984	10	6	Krick & Bernstein (2007)
20.	A141	10	4	Krick & Bernstein (2007)
21.	AC 114	11	2	Krick & Bernstein (2007)
22.	AC 118	14	5	Krick & Bernstein (2007)

[a]Krick & Bernstein (2007) measured these $f_{\rm ICS}$ values in the r band.

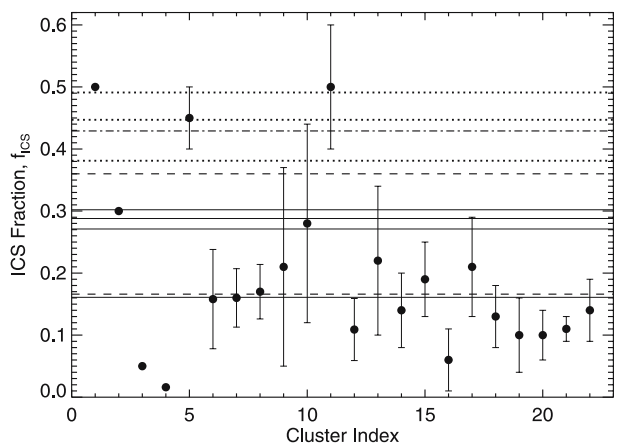

Figure 6. Fraction $f_{\rm ICS}$ of intracluster stars. The horizontal lines show the average $f_{\rm ICS}$ values in our simulations, from the runs of the series in Table 1 (section 4), with *solid line*: Virgo-like cluster (series A–D), *dashed line*: Perseus-like cluster (series E–F), *dotted line*: NFW model cluster (series G–I), *dot-dashed line*: Perseus-like growing cluster (series J). The symbols and error bars show actual measurements, as tabulated in Table 12.

One free parameter is the geometric factor in equation (10), but for reasonable density profiles, the values of that factor do not appear to vary much. The assumption that a galaxy is considered 'tidally disrupted' if 50% of its mass becomes unbound is also the most reasonable one we could make. Our technique for generating the initial conditions is based on four key assumptions:

(1) the galaxy distributions are isotropic,
(2) the galaxy number density profile $\nu(r)$ follows the density profile $\rho_{\rm halo}(r)$ of the background cluster halo,
(3) the mass is segregated in the cluster, with the most massive galaxies being located in the center, and
(4) the cluster is in equilibrium (except for series J).

So even though our prescription for generating the initial conditions contains many tunable parameters, we believe that the underlying approach is sound.

On the negative side, two particular aspects of the methodology can be considered weak. First, the treatment of galaxy harassment is highly speculative. We have assumed that some amount of orbital kinetic energy ΔE is dissipated into internal energy during an encounter between two galaxies, that this amount is related to the initial internal energies of the galaxies, and that the energy dissipated is distributed equally between the two galaxies. The dissipation of energy and its consequences during a real galactic encounter are certainly much more complex. The implemented subgrid model could thus, potentially, be refined.

Another important limitation of our approach is that it deals with isolated clusters in equilibrium (except for series J). In the real universe, clusters constantly experience mergers and accretion. We justify our approach by the fact that most clusters will experience, at some epoch, a *major merger*, during which most of the final mass of the cluster is assembled. From that point, if we can neglect the addition of mass by minor mergers and accretion, the cluster can be treated as isolated. Of course, such scenario cannot describe all clusters. In a forthcoming paper (Brito *et al.* 2008), we will present a study of cluster formation and evolution inside a cosmological volume containing many clusters. This will be achieved by implementing the subgrid approach described in this paper into a cosmological N-body algorithm.

6. Summary and conclusion

We have designed a simple model for the evolution of galaxies in an isolated cluster, in order to compare the destruction of dwarf galaxies by mergers *vs.* tidal disruptions, and to predict the contribution of DGs to the origin of intracluster stars. Our algorithm combines a direct N-body computation of gravitational interactions, along with a subgrid treatment of the other physical processes (merger, tidal disruption, accretion, etc.) of the galaxies. Using this algorithm, we have performed a total of 148 numerical simulations of galaxy clusters, examining the fate of DGs. Our results and conclusions are as follows:

- The destruction of dwarf galaxies by mergers dominates over destruction by tides, in most of our simulation runs with all the models (β-Virgo, β-Perseus, NFW) of cluster halo density.

- The destruction of galaxies by the tidal field of other galaxies and by the cluster halo imparts a significant amount of galactic mass into the ICM. This is sufficient to account for the observed fraction of intracluster light in galaxy clusters. In our simulations, the average ICS luminosity fraction, $f_{\rm ICS}$, has a range 16–49%. We see a clear trend of increase of $f_{\rm ICS}$ with the mass of the cluster halo. All these are well consistent with observations and other numerical studies.
- In the NFW model simulated clusters, there are a large number of tidal disruptions of galaxies caused by the gravitational potential of the cluster halo, and this component dominates the mass fraction. We note that it has been our assumption that the cluster halo is stationary, and does not evolve in response to the forces exerted on it by the galaxies (section 2.1). Such an assumption is probably a poor one with the NFW model clusters. We point out that this could imply a possible solution to the cusp crisis of cluster dark matter halos. The central cuspy region of the cluster dark matter halo could have inelastic encounters with the member galaxies, which could inject energy into the halo and erase the cusp.
- In our simulations, the presence of a cD galaxy increases occurrences of accretion, decreases tidal disruptions by the cluster halo, and reduces the ICS luminosity fraction. This is opposite to the trend seen from observations that $f_{\rm ICS}$ is higher in the presence of a cD.
- The vast majority of galaxies destroyed by tides are dwarfs. However, a few high-mass ($M > 10^{11}{\rm M}_{\odot}$) galaxies are also destroyed, and these can provide a substantial fraction of the ICL. Furthermore, the destruction of such high mass galaxies is required, since the dwarfs alone do not contain enough stars to account for the observed ICL, even if they were all destroyed.

Acknowledgements

This work benefited from stimulating discussions with L. Edwards and C. Robert. We thank John Kormendy for useful correspondence. All calculations were performed at the Laboratoire d'astrophysique numérique, Université Laval. We thank the Canada Research Chair Program and NSERC for support.

Appendix

The internal energy of galaxies

Since we represent galaxies as individual particles, we cannot directly compute their internal energy. We therefore need an estimate that can then be used in equation (10). We write the potential energy of a galaxy of mass M and radius R as:

$$W = -\frac{\zeta G M^2}{R}, \tag{29}$$

where ζ is the *geometric factor*, which depends on the shape and density distribution of the galaxy. For a uniform-density sphere, $\zeta = 3/5$. In our simplified model, we treat galaxies as spheres, but we should certainly not assume a uniform density. Instead, any galaxy will be centrally concentrated. The value of ζ will depend on the assumed density profile, but we do not expect that dependence to be very strong if we stick with

reasonable profiles. So we consider the simplest case of an isothermal sphere with a cut-off radius R. The density and mass inside r are given by:

$$\rho(r) = \frac{M}{4\pi R r^2}, \tag{30}$$

$$m(r) = \frac{Mr}{R}, \tag{31}$$

where $M \equiv m(R)$ is the total mass. The gravitational field is given by:

$$\mathbf{g} = -\nabla\phi = -\frac{Gm(r)}{r^2}\hat{r} = -\frac{GM}{rR}\hat{r}. \tag{32}$$

We integrate this expression, with the boundary condition $\phi(R) = -GM/R$, to get the gravitational potential,

$$\phi = \frac{GM}{R}\left(\ln\frac{r}{R} - 1\right). \tag{33}$$

The potential energy is given by:

$$\begin{aligned} W &= \frac{1}{2}\iiint \phi(r)\rho(r)d^3r \\ &= \frac{GM^2}{2R^2}\int_0^R \left(\ln\frac{r}{R} - 1\right)dr \\ &= -\frac{GM^2}{R}. \end{aligned} \tag{34}$$

Hence, $\zeta = 1$ for an isothermal sphere. Interestingly, this is not much different from the value of 3/5 for a uniform sphere. This supports our claim that the sensitivity of ζ on the density profile is weak. For the kinetic energy, we assume that the galaxies are virialized. Hence, $K = -W/2$, and therefore the internal energy is given by:

$$U = K + W = -\frac{GM^2}{2R}. \tag{35}$$

References

Aguerri, J. A. L. *et al.* 2005, *AJ*, **129**, 2585.
Arabadjis, J. S., Bautz, M. W., Garmire, G. P. 2002, *ApJ*, **572**, 66.
Arnaboldi, M. *et al.* 2003, *AJ*, **125**, 514.
Arnaboldi, M. 2004, *IAUS*, **217**, 54.
Bernstein, G. M., Nichol, R. C., Tyson, J. A., Ulmer, M. P., Wittman, D. 1995, *AJ*, **110**, 1507.
Bothun, G. D. *et al.* 1991, *ApJ*, **376**, 404.
Brainerd, T. G., Specian, M. A. 2003, *ApJ*, **593**, L7.
Brito, W., Barai, P., Martel, H. 2009, in preparation.
Carlberg, R. G. *et al.* 1997, *ApJ*, **485**, L13.
Castro-Rodriguez, N., Aguerri, J. A. L., Arnaboldi, M., Gerhard, O., Freeman, K. C., Napolitano, N. R., Capaccioli, M. 2003, *A&A*, **405**, 803.
Cavaliere, A., Fusco-Femiano, R. 1976, *A&A*, **49**, 137.

Cellone, S. A., Buzzoni, A. 2005, *MNRAS*, **356**, 41.
Côté, S., Freeman, K. C., Carignan, C., Quinn, P. J. 1997, *AJ*, **114**, 1313.
De Propris, R. *et al.* 2003, *MNRAS*, **342**, 725.
Drinkwater, M. J. *et al.* 2003, *Nature*, **423**, 519.
Ettori, S. 2003, *MNRAS*, **344**, L13.
Feldmeier, J. J., Mihos, J. C., Morrison, H. L., Harding, P., Kaib, N., Dubinski, J. 2004a, *ApJ*, **609**, 617.
Feldmeier, J. J., Ciardullo, R., Jacoby, G. H., Durrell, P. R. 2004b, *ApJ*, **615**, 196.
Gal-Yam, A. *et al.* 2003, *AJ*, **125**, 1087.
Gerhard, O. *et al.* 2005, *ApJ*, **621**, L93.
Girardi, M., Giuricin, G., Mardirossian, F., Mezzetti, M., Boschin, W. 1998, *ApJ*, **505**, 74.
Gonzalez, A. H., Zabludoff, A. I., Zaritsky, D., Dalcanton, J. J. 2000, *ApJ*, **536**, 561.
Gonzalez, A. H., Zabludoff, A. I., Zaritsky, D. 2005, *ApJ*, **618**, 195.
Gonzalez, A. H., Zaritsky, D., Zabludoff, A. I. 2007, preprint (arXiv0705.1726).
Grebel, E. K. 2001, *ASPC*, **239**, 280.
Gregg, M. D., West, M. J. 1998, *Nature*, **396**, 549.
Jordan, A., Côté, P., West, M. J., Marzke, R. O., Minniti, D., Rejkuba, M. 2004, *AJ*, **127**, 24.
Karachentseva, V. E., Karachentsev, I. D., Boerngen, F. 1985, *A&AS*, **60**, 213.
King, I. 1962, *AJ*, **67**, 471.
Krick, J. E., Bernstein, R. A., Pimbblet, K. A. 2006, *AJ*, **131**, 168.
Krick, J. E., Bernstein, R. A. 2007, *AJ*, **134**, 466.
Lee, H. *et al.* 2003, *AJ*, **125**, 2975.
Lewis, I. *et al.* 2002, *MNRAS*, **334**, 673L.
Lin, Y.-T., Mohr, J. J. 2004, *ApJ*, **617**, 879.
Makino, N., Sasaki, S., Suto, Y. 1998, *ApJ*, **497**, 555.
Martel, H. 1991, *ApJ*, **377**, 7.
Mateo, M. L. 1998, *ARA&A*, **36**, 435.
Maughan, B. J., Jones, C., Jones, L. R., Van Speybroeck, L. 2007, *ApJ*, **659**, 1125.
Mieske, S., Hilker, M., Jordan, A., Infante, L., Kissler-Patig, M. 2007, preprint (arXiv:0706.2724).
Mihos, J. C., Harding, P., Feldmeier, J., Morrison, H. 2005, *ApJ*, **631**, L41.
Miller, G. E. 1983, *ApJ*, **268**, 495.
Moore, B., Katz, N., Lake, G., Dressler, A., Oemler, A. 1996, *Nature*, **379**, 613.
Murante, G. *et al.* 2004, *ApJ*, **607**, L83.
Napolitano, N. R. *et al.* 2003, *ApJ*, **594**, 172.
Navarro, J. F., Frenk, C. S., White, S. D. M. 1997, *ApJ*, **490**, 493.
Oegerle, W. R., Hill, J. M. 2001, *AJ*, **122**, 2858.
Piffaretti, R., Kaastra, J. S. 2006, *A&A*, **453**, 423.
Pratt, G. W., Arnaud, M. 2005, *A&A*, **429**, 791.
Quintana, H., Lawrie, D. G. 1982, *AJ*, **87**, 1.
Rudick, C. S., Mihos, J. C., McBride, C. 2006, *ApJ*, **648**, 936.
Ryan, R. E. Jr. *et al.* 2007, *ApJ*, **668**, 839.
Sandage, A., Binggeli, B., Tammann, G. A. 1985, *AJ*, **90**, 1759.
Schechter, P. 1976, *ApJ*, **203**, 297.
Schombert, J. M. 1988, *ApJ*, **328**, 475.
Sommer-Larsen, J. *et al.* 2005, *MNRAS*, **357**, 478.
Spergel, D. N. *et al.* 2007, *ApJS*, **170**, 377.
Thompson, L. A., Gregory, S. A. 1993, *AJ*, **106**, 2197.
Tyson, J. A., Fischer, P. 1995, *ApJ*, **446**, L55.
Wechsler, R. H., Bullock, J. S., Primack, J. R., Kravtsov, A. V., Dekel, A. 2002, *ApJ*, **568**, 52.
West, M. J. *et al.* 1995, *ApJ*, **453**, L77.
White, S. D. M., Navarro, J. F., Evrard, A. E., Frenk, C. S. 1993, *Nature*, **366**, 429.
White, P. M., Bothun, G., Guerrero, M. A., West, M. J., Barkhouse, W. A. 2003, *ApJ*, **585**, 739.
Willman, B., Governato, F., Wadsley, J., Quinn, T. 2004, *MNRAS*, **355**, 159.
Yang, X., Mo, H. J., van den Bosch, F. C. 2003, *MNRAS*, **339**, 1057.
Zibetti, S., White, S. D. M., Schneider, D. P., Brinkmann, J. 2005, *MNRAS*, **358**, 949.
Zwicky, F. 1951, *PASP*, **63**, 61.